

©2019 IEEE. Personal use of this material is permitted. Permission from IEEE must be obtained for all other uses, in any current or future media, including reprinting/republishing this material for advertising or promotional purposes, creating new collective works, for resale or redistribution to servers or lists, or reuse of any copyrighted component of this work in other works.

# Deep Morphological Hit-or-Miss Transform Neural Network

Muhammad Aminul Islam, *Member, IEEE*, Bryce Murray, *Student Member, IEEE*, Andrew Buck, *Member, IEEE*, Derek T. Anderson, *Senior Member, IEEE*, Grant Scott, *Senior Member, IEEE*, Mihail Popescu, *Senior Member, IEEE*, James Keller, *Life Fellow, IEEE*,

**Abstract**—Neural networks have demonstrated breakthrough results in numerous application domains. While most architectures are built on the premise of convolution, alternative foundations like morphology are being explored for reasons like interpretability and its connection to the analysis and processing of geometric structures. Herein, we investigate new deep networks based on the morphological hit-or-miss transform. The hit-or-miss takes into account both foreground and background when measuring the fitness of a target shape in an image. We identify limitations of current hit-or-miss definitions, and we formulate an optimization problem to learn the transform. Our analysis shows that convolution, in fact, acts like a hit-miss transform through semantic interpretation of its filter differences. Analogous to the generalized hit-or-miss transform, we also introduce an extension of convolution and show that it outperforms conventional convolution on benchmark data sets. We conducted experiments on synthetic and benchmark data sets, and we show that the direct encoding hit-or-miss transform provides better interpretability on learned shapes consistent with objects whereas our morphologically inspired generalized convolution yields higher classification accuracy.

**Index Terms**—Deep learning, morphology, hit-or-miss transform, convolution, convolutional neural network

## I. INTRODUCTION

Deep learning has demonstrated robust predictive accuracy across a wide range of applications. Notably, it has achieved and, in some cases, surpassed human-level performance in many cognitive tasks, for example, object classification, detection, and recognition, semantic and instance segmentation, and depth prediction. This success can be attributed in part to the ability of a *neural network* (NN) to construct an arbitrary and very complex function by composition of simple functions, thus empowering it as a formidable machine learning tool.

To date, state-of-the-art deep learning algorithms mostly use convolution as their fundamental operation, thus the name *convolutional neural network* (CNN). Convolution has a rich and proud history in signal/image processing, for example extracting low-level features like edges, noise filtering (low/high pass filters), frequency-orientation filtering via the Gabor, etc. In a continuous space, it is defined as the integral of two functions—an image and a filter in the context of image processing—after one is reversed and shifted, whereas in discrete space, the integral realized via summation. CNNs

Muhammad Aminul Islam, Bryce Murray, Andrew Buck, Derek T. Anderson, Grant J. Scott, Mihail Popescu, and James Keller are with the Department of Electrical Engineering and Computer Science, University of Missouri, Columbia, MO 65211, USA. E-mail: (mig5g@missouri.edu).

progressively learn more complex features in deeper layers with low level features such as edges in the earlier layers and more complex shapes in the later layers, which are composite of features in the previous layer. One strong argument against convolution is that its filter does not lend itself to interpretable target shape. Because convolution is correlation with a time/spatial reversed filter, the filter weights do not necessarily indicate the absolute intensities/levels in shape. Instead, they signify relative importance. Recently, some studies like guided backpropagation [1] and saliency mapping [2] aim to explain a CNN. However, their explanations depends on an input image and the learned filters. The filters alone do not explain the learned model.

In contrast to convolution, morphology-based operations are interpretable—though they have only been lightly studied and explored in the context of deep neural networks [3]–[15]. Morphology is based on set theory, lattice theory, topology and random functions and has been used for the analysis and processing of geometric structures [16]–[25]. The most fundamental morphological operations are erosion and dilation, which can be combined to build more complex operations such as opening, closing, morphological gradient, and the hit-or-miss transform. Grayscale erosion and dilation are used to find the minimal offset by which the foreground and background of the target pattern fits in an image, thus providing an absolute measure of fitness in contrast to relative measure by convolution and facilitating the learning of interpretable SEs.

Recently, a few deep neural networks have been proposed based on morphological operations such as dilation, erosion, opening, and closing [3], [26]. In [3], Mellooli et al. explored pseudo-dilation and pseudo-erosion defined in terms of weighted counter harmonic mean, which can be carried out as the ratio of two convolution operations. However, their network is not an end-to-end morphological network, rather a hybrid of traditional convolution and pseudo-morphological operations. In [26], Nogueira et al. proposed a neural network based on binary *structuring element* (SE) consisting of 1s and 0s indicating which pixels are relevant to the target pattern. Their proposed implementation to realize this binary SE requires a large number of parameters, specifically  $s^2$  binary filters of size  $s \times s$  just to represent a single  $s \times s$  SE; which makes this method expensive in terms of storage and computation and not suitable for deep learning. Furthermore, they did not conduct any experiments nor provide results for popular computer vision benchmark datasets (e.g., MNIST or Cifar). More importantly, none of these algorithms

simultaneously apply dilation and erosion on an image to take into account both foreground and background. In the morphological community, there is a well-known operation for doing this, called the hit-miss transform.

Following the success of convolution based shared weight neural networks on handwritten digit recognition tasks in 1990, Gader et al. introduced a generalized hit-or-miss transform network, referred to as image algebra network [27]. Later, standard hit-or-miss transform was applied in target detection [6]. All of these methods employed two SEs, one for the hit to find the “fitness” of an image relative to target foreground and another for the miss to find the “fitness” relative to target background. However, existing definitions do not include the condition that the intersection of the hit and miss SEs must be empty. Failing to meet this condition can result in semantically inconsistent and uninterpretable SEs. In order to handle this issue, we put forth an optimization problem enforcing the non-intersecting condition.

However, considering only foreground and background are not sufficient to describe a target shape. We also need *Don’t Care* (DNC), which denotes regions of the SE that are not relevant to detecting a target pattern. While binary morphology considers 0s as DNCs and it ignores them during computation, its grayscale extension unfortunately considers all elements including 0s. Therefore, we propose a new extension to the hit-or-miss transform which allows it to describe a grayscale shape in terms of relevant and non-relevant elements (i.e., DNC). Furthermore, we provide the conditions that will make elements under the conventional definition of hit-or-miss to act as DNC and we show that the valid ranges for target and DNC elements are discontinuous. This constraint poses a challenge to data-driven learning using gradient descent, which requires the variables to reside in a (constrained or unconstrained) continuous space. As a result, we propose hit-or-miss transforms that implicitly enforces non-intersecting condition and addresses DNC.

Last, while convolution can act like a hit-or-miss transform – when its “positive filter weights” correspond to foreground, “negative weights” to background, and 0s for DNC – it differs in some important aspects. For example, elements in a hit-or-miss SE indicate the absolute intensity levels in the target shape whereas weights in a convolution filter indicate relative levels/importance. Another difference is that the sum operation gives equal importance to all operands versus max (or min) in the hit-or-miss transform. Motivated by the introduction of the generalized hit-or-miss, we propose extensions of convolution, referred to as generalized convolution hereafter, by replacing the sum with the generalized mean. The use of a parametric generalized mean allows one to choose how values in the local neighborhood contribute to the result; e.g., all contribute equally (as in the case of the mean) or just one drives the result (as in max), or something in between. Through appropriate selection of this parameter, performance can be significantly enhanced as demonstrated by our experiments.

While convolution, likewise the hit-or-miss transform, consider foreground, background, and DNC, they different in how fitness is evaluated. For example, convolution uses a relative measure while the hit-or-miss uses an absolute measure. One

question naturally arises, how does this difference impact performance on two aspects of a learned model, explainability and accuracy. Our analysis shows that morphology provides better interpretability through its use of an absolute measure, while convolution yields higher accuracy as a relative measure is more robust.

Our article makes the following contributions.

- We identify limitations in the current definition of the grayscale hit-or-miss and we formulate an optimization to properly learn the transform in a neural network.
- In light of this optimization, we propose an algorithm to learn the hit-or-miss transform and also its generalization.
- We extend “conventional convolution” used in most neural networks by substituting the sum operation with a parametric generalized mean.
- Synthetic and benchmark data sets are used to show the behavior and effectiveness of the proposed theories in a quantitative and qualitative respect.

The remainder of this article is organized as follows. In Section II, we provide notations and definitions of binary and grayscale morphological operations. Section III introduces the optimization problem, learning algorithm, our generalization of the hit-or-miss transform, and our extension of convolution, followed by experiments and results in Section IV.

## II. BINARY AND GRayscale MORPHOLOGY

First, we briefly go over definitions related to binary morphology in order to understand the basis of morphological operations and their semantic meaning pertaining to image processing. The most basic of morphological operations are dilation and erosion, which coupled with algebraic operations (e.g., sum) can create more complex morphological operations such as opening, closing, hit-or-miss transform, top-hat, thinning, thickening, and skeleton, to name a few.

### A. Binary Morphology

Binary morphology is grounded in the theory of sets. Let  $Z$  be a set of integers.

**Definition 1. (Dilation)** Let  $A$  be an image,  $B$  a SE, and  $A, B \in Z^2$ . The dilation of  $A$  by  $B$ , denoted by  $A \oplus B$  is

$$A \oplus B = \{z | (\hat{B})_z \cap A \neq \emptyset\},$$

where  $\hat{B}$  is the reflection of  $B$  about its origin and  $(B)_z$  is the translation of  $B$  by  $z$  [28], [29].

As the above definition shows, the dilation operation involves reflecting  $B$  and then shifting the reflected  $B$  by  $z$ . The dilation of  $A$  by  $B$  is the set of all displacements  $z$  such that  $B$  and  $A$  overlap by at least one element. The set  $B$  is often referred to as the *structuring element* (SE).

**Definition 2. (Erosion)** Let  $A$  be an image,  $B$  a SE, and  $A, B \in Z^2$ . Then the erosion of  $A$  by  $B$ , denoted  $A \ominus B$  is

$$A \ominus B = \{z | (B)_z \subseteq A\},$$

where  $(B)_z$  is translation of  $B$  by  $z$  [28], [29].

The above equation indicates that  $A \ominus B$  is the set of all points such that  $B$ , translated by  $z$ , is contained in  $A$ .

SEs can be “non-flat”, when the weights are non-uniform or flat when the weights are uniform. With “flat” SEs, particularly when elements are zeros, dilation is the maximum of the image pixels values in the window erosion is the minimum in the window. Thus, dilation and erosion become order statistics with flat structuring elements.

It is a well-known fact that dilation and erosion are duals of each other with respect to complement and reflection.

$$(A \ominus B)^c = A^c \oplus \hat{B},$$

where  $A^c$  is the complement of  $A$ . Similarly,

$$(A \oplus B)^c = A^c \ominus \hat{B}.$$

The morphological hit-or-miss transform is a technique for shape detection that simultaneously matches both foreground and background shapes in an image.

**Definition 3. (Binary Hit-or-Miss)** The binary hit-or-miss transform w.r.t. SEs  $H$  and  $M$  satisfying  $H \cap M = \emptyset$  is

$$A \odot (H, M) = (A \ominus H) \cap (A^c \ominus M),$$

where  $H$  is the set associated with the foreground or an object and  $M$  is the set of elements associated with the corresponding background.

In this way,  $A \odot (H, M)$  finds all the points (origins of the translated structuring elements) at which, simultaneously,  $H$  found a match (“hit”) in  $A$  and  $M$  found a match in  $A^c$ . By using the dual relationship between erosion and dilation, the hit-or-miss transform equation can alternatively be written as

$$A \odot B = (A \ominus H) \setminus (A \oplus M), \quad (1)$$

where  $\setminus$  is the set difference operation ( $A \setminus B = A \cap B^c$ ).

Though obvious from Def. 3, we emphasize that the intersection of sets that define the foreground (aka hit) and background (aka miss) must be null or empty, i.e., both  $H(x, y)$  and  $M(x, y)$  at a given location  $(x, y)$  cannot be 1. This is because an element in the target structure can either be treated as foreground, background or DNC (an element not part of the target structure and is defined by 0s in both hit and miss SEs) but it cannot simultaneously be foreground and background. We illustrate all these cases (e.g., non-intersecting and intersecting SEs) with examples in Fig. (1). Table I shows combination of hit-miss values for binary morphology.

TABLE I: Binary combinations for the hit-or-miss transform in binary morphology

H	M	Semantic meaning
0	0	DNC
0	1	Background
1	0	Foreground
1	1	Inadmissible - semantically infeasible

### B. Grayscale Morphology

Let  $f$  be a grayscale image,  $b$  a structuring element, and  $f(x, y)$  the grayscale intensity at a location  $(x, y)$ .

**Definition 4. (Grayscale Dilation)** The grayscale dilation of  $f$  by  $b$ , denoted as  $f \oplus b$ , is [28]

$$(f \oplus b)(x, y) = \max\{f(s - x, t - y) + b(x, y) \mid (s - x, t - y) \in D_f; (x, y) \in D_b\}, \quad (2)$$

where  $D_f$  and  $D_b$  are the domains of  $f$  and  $b$ , respectively.

On a side note, there is a parallel between 2-D convolution and dilation, when sum replaces product and when max replaces sum.

**Definition 5. (Grayscale Erosion)** The grayscale erosion of  $f$  by  $b$ , denoted as  $f \ominus b$ , is defined as

$$(f \ominus b)(x, y) = \min\{f(s + x, t + y) - b(x, y) \mid (s + x, t + y) \in D_f; (x, y) \in D_b\}, \quad (3)$$

where  $D_f$  and  $D_b$  are the domains of  $f$  and  $b$ , respectively [28].

On a side note, there is a parallel between 2-D correlation and erosion, when sum replaces product and when min replaces sum.

As noted in [27], [29], the umbra transform provides the theoretical basis for grayscale extension for morphological operation by providing a mechanism to express grayscale operations in terms of binary operations. Interested readers can refer to [27], [29] for the theory and proof of the extension.

A major difference between binary and grayscale morphology is that unlike binary morphological operations, there is no explicit DNC conditions in grayscale morphology, i.e., all elements including those with 0s contribute to the results. So, a mechanism needs to be put in place to distinguish between target pixels and DNC. Ideally, the DNC elements can be specified by  $-\infty$ , which would result in maximum value for the erosion and minimum value for the dilation and thus will never contribute to the result. While suitable for hand-crafted SE design, it might not be feasible to learn  $-\infty$ -valued elements in the context of data-driven learning unless some constraints are imposed. Instead, the SEs can be designed such that some of the elements can act as DNC by setting those elements to a very low value compared to neighborhood elements such that the difference is always high and as such it never carries over to the result. Thus, the filters can be designed smartly so that DNC is automatically enforced via appropriate selection of values. Alternatively, the erosion equation can be rewritten to consider only the foreground elements as in binary morphology.

Next, we find the condition for an element in an erosion SE to act as DNC. Let  $I$  be an image in the interval  $[lb_I, ub_I]$ . Furthermore, let  $h$  be the erosion SE with foreground elements in the interval  $[lb_{h_f}, ub_{h_f}]$  and DNC elements in the interval,  $[lb_{h_d}, ub_{h_d}]$ . Then the maximum value possible for foreground is  $v_{max} = ub_I - lb_{h_f}$ . We want the DNC to produce higher than  $v_{max}$  for the lowest image value,  $lb_I$ . This gives us  $lb_I - d \geq v_{max}$  or  $d \leq lb_I - ub_I + lb_{h_f}$ , where  $d$  is a DNC element.

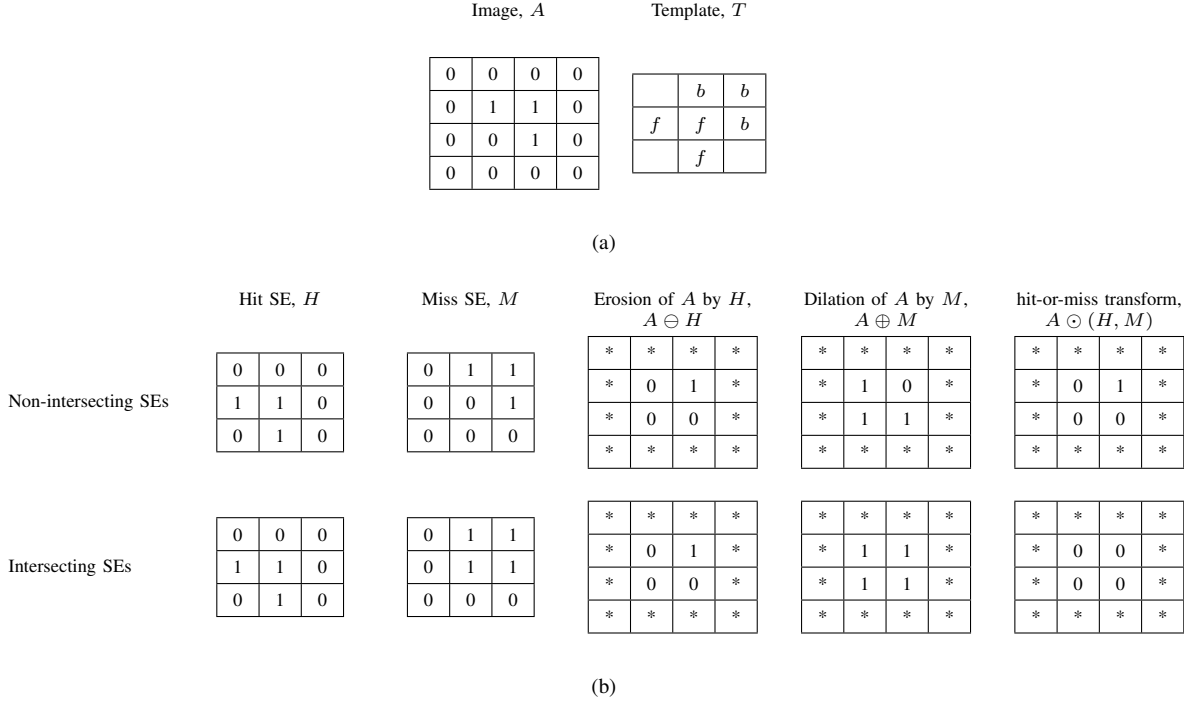


Fig. 1: Example of binary hit-or-miss transform to detect a top-right corner. (a) shows a binary image,  $A$ , with a top-right corner in the top-right  $3 \times 3$  window and a  $3 \times 3$  template,  $T$ , that encodes the structure of the top-right corner and is used to construct SEs for hit-or-miss transform,  $f$  stands for foreground,  $b$  for background and empty cells are DNC. (b) Top row shows hit-or-miss transform for non-intersecting SEs derived from  $T$ , which correctly finds matching for both foreground in hit (1 in erosion means the foreground is matched) and background in miss (0 in dilation means the background is matched). Bottom row shows intersecting SEs, which produces empty set as it cannot find a matching for both foreground and background. Note that the transform is calculated without padding of the input image so the output size is 2 by 2.

Consequently,  $ub_{h_d} = lb_I - ub_I + lb_{h_f}$  and  $lb_{h_d} = -\infty$ . Since  $lb_I - ub_I < 0$  for a grayscale image,  $ub_{h_d} < lb_{h_f}$ . This reveals that there is a discontinuity between valid ranges for foreground and DNC elements, i.e., a separation of  $ub_I - lb_I$  must exist between them. This poses a challenge to the data-driven learning tasks since the weights learned are real-valued in a continuous domain and discontinuity cannot be enforced. Similar analysis can be done for dilation SE, which also gives a similar condition.

The hit-or-miss transform for grayscale is defined in literature in terms of Eq. (1), by replacing the set difference operation with an arithmetic subtraction operation.

**Definition 6. (Grayscale Hit-or-Miss Transform)** The grayscale hit-or-miss transform is

$$f \odot (h, m) = (f \ominus h) - (f \oplus m^r),$$

where  $m^r$  is the reflection of  $m$ , i.e.,  $m^r(x, y) = m(-x, -y)$ , which gives

$$\begin{aligned} (f \odot (h, m))(x, y) &= \min \{(f(x+a, y+b) - h(a, b)) | \\ &(x+a, y+b) \in D_f; a, b \in D_h\} \\ &- \max_{a, b \in D_m} \{(f(x+a, y+b) + m(a, b)) \\ &(x+a, y+b) \in D_f; a, b \in D_m\}, \end{aligned}$$

where  $(x+a, y+b) \in D_f$  and  $D_f$ ,  $D_h$ , and  $D_m$  are the domains of  $f$ ,  $h$ , and  $m$ , respectively [28].

Let  $h$  and  $m$  be SEs with non-negative weights. The hit and miss SEs together defines the target pattern with hit indicating the foreground and miss SE indicating the background. For example, if  $h(x, y) > m(x, y)$  at a location  $(x, y)$  - then that pixel is treated more as foreground than background and vice versa.

Similar to the binary case, the filters must be non-intersecting, i.e., satisfy the following constraints,

$$h(x, y) \leq m^c(x, y) \text{ or } m(x, y) \leq h^c(x, y)$$

where  $h^c$  and  $m^c$  are the complement of  $h$  and  $m$ , respectively. This condition prevents the hit and miss SEs from contradicting each other. According to this condition, if  $h(x, y) = 0.9$ , then  $m(x, y)$  must be less than  $1 - 0.9$  or  $0.1$  for an unit interval image.

### C. Properties of morphological operations

Both grayscale erosion and dilation as well as the hit-or-miss transform are translation invariant, i.e.,

$$(f + c) \ominus b = f \ominus b + c \text{ and}$$

$$(f + c) \oplus b = f \oplus b + c,$$

where  $c$  is an arbitrary value. Note that these operations as seen from Eqs. (2) and (3) are not scale invariant. In contrast, convolution is scale invariant but not translation invariant.

No DNC Vs. DNC - Case I				No DNC Vs. DNC - Case II				Non-intersecting vs. Intersecting SEs			
Grayscale image, $f$	0.0	0.0	0.3	0.3	0.0	0.0	0.0	0.0	0.0	0.0	0.0
	0.0	0.7	0.7	0.3	0.0	1.0	1.0	0.0	0.0	1.0	0.0
	0.0	0.0	0.7	0.0	0.0	0.0	1.0	0.0	0.0	0.0	1.0
	0.0	0.0	0.0	0.0	0.0	0.0	0.0	0.0	0.0	0.0	0.0
Hit SE, $h$	0.0	0.0	0.0	$-\infty$	$-\infty$	$-\infty$	$-\infty$	0.0	0.1	0.1	$-\infty$
	0.7	0.7	0.0	0.7	0.7	0.0	$-\infty$	0.7	0.7	0.1	0.7
	0.0	0.7	0.0	$-\infty$	0.7	$-\infty$	$-\infty$	$-\infty$	0.7	$-\infty$	$-\infty$
Miss SE, $m$	0.0	0.7	0.7	$-\infty$	0.7	0.7	$-\infty$	0.0	0.7	0.7	0.1
	0.0	0.0	0.7	$-\infty$	$-\infty$	0.7	$-\infty$	0.0	0.1	0.1	0.1
	0.0	0.0	0.0	$-\infty$	$-\infty$	$-\infty$	$-\infty$	$-\infty$	0.1	$-\infty$	$-\infty$
Erosion of $f$ by $h$ , $f \ominus h$	*	*	*	*	*	*	*	*	*	*	*
	*	-0.7	0.0	*	*	-0.7	0.0	*	*	-0.7	-0.1
	*	-0.7	-0.7	*	*	-0.7	-0.7	*	*	-0.7	-0.7
	*	*	*	*	*	*	*	*	*	*	*
Dilation of $f$ by $m$ , $f \oplus m$	*	*	*	*	*	*	*	*	*	*	*
	*	1.4	1.0	*	*	1.4	1.0	*	*	1.7	1.1
	*	1.4	1.4	*	*	1.4	1.4	*	*	1.7	1.7
	*	*	*	*	*	*	*	*	*	*	*
hit-or-miss transform, $f \odot (h, m)$	*	*	*	*	*	*	*	*	*	*	*
	*	-2.1	-1.0	*	*	-2.1	-1.0	*	*	-2.4	-0.4
	*	-2.1	-2.1	*	*	-2.1	-2.1	*	*	-2.4	-2.4
	*	*	*	*	*	*	*	*	*	*	*
Comments	SEs with and without DNC produce the same results when the SE including its 0s exactly fit in the image, $f$ . SEs with and without DNC produce the same results as expected.				SE with DNC considers only foreground and background elements and yields better results.				Non-intersecting SEs are unable to find a match for both foreground and background structures.		

Fig. 2: Grayscale hit-or-miss transform illustrating the importance of DNC and non-intersecting condition with an example of top-right corner detection. In SEs,  $-\infty$  is used for DNC. The first two columns show the case when the SEs including its 0s exactly fit in the image,  $f$ . SEs with and without DNC produce the same results as expected. Third and fourth columns are for the case where SEs for hit and miss fit below and above, respectively in the target area (top-right  $3 \times 3$  window) of the input image. Without DNC, 0s (vs. 0.7) in  $h$  determine the output, which remains the same even though the input image is changed. On the other hand, with DNC, the output latches on 0.7s, not on 0s in  $h$  and varies with the change in input. Fifth and sixth columns compare the effect of non-intersecting and intersecting SEs. In the sixth column, erosion of  $f$  by intersecting SE  $h$  produces  $-0.7$  for all cells, meaning no matching foreground-pattern found in any window of the input image.

### III. METHODS

#### A. Morphological Shared Weight Neural Network

Inspired by the success of shared weight CNNs on handwritten digit recognition (MNIST dataset) by LeCun in 1990 [30], Gader et al. [27] introduced morphology based image algebra network substituting convolution for morphological operations. Particularly, they used the hit-or-miss transform because of its ability to take into account both background and foreground of an object. This transform was extended with a power mean to soften the extremely sensitive max and min operations, where all the parameters including the exponents of the power mean were learned. In later works, Won et. al. [5] and Khabou et al. [31] used the standard hit-or-miss transform. None of these works considered the following aspects of hit-or-miss transform, non-intersecting condition and DNC. As illustrated with examples of binary and grayscale morphology in Figs. 1 and 2, DNC plays an important role in the design of an SE that helps disregard irrelevant parts of an image not necessary for finding a target pattern while keeping focus only

on the relevant parts. Without a mechanism in place to provide for DNC, each element will be treated as a part of the target pattern and contribute to the output even if they are not. This can hurt the performance when there is a lot of variation in context and object shape and size, however they still might perform well for rigid pattern with fixed size and shape with little change in background and foreground.

Figure 2 illustrates the role of non-intersecting condition and DNC in the grayscale hit-or-miss transform. Considering these conditions, we propose the following hit-or-miss transform

$$(f \odot (h, m))(x, y) = \min_{a, b \in D_{h_f}} (f(x + a, y + b) - h(a, b)) - \max_{a, b \in D_{m_b}} (f(x + a, y + b) + m(a, b)), \quad (4)$$

subject to

$$h(a, b) \geq m^c(a, b), \text{ or } m(a, b) \geq h^c(a, b),$$

where  $x + a, y + b \in D_f$ ,  $h^c(a, b)$  and  $m^c(a, b)$  are complements of  $h$  and  $m$ , and  $h_f \subseteq h$  and  $m_b \subseteq m$  are the foreground

and background elements in  $h$  and  $m$ , respectively. We remark that SEs learned without non-intersection condition may turn out to preserve this property, however it cannot be guaranteed so we make this condition explicit in our proposed definition.

### B. Hit-or-Miss Transform Neuron:

A major challenge in enforcing the non-intersecting condition via complement according to Eq. (4) is computing the ranges for image and SEs. This is because the ranges can be at different scales and can vary across layers and from one iteration to the next due to updating of elements during optimization. To circumvent this issue, we take a more restrictive approach (analogous to binary morphology) where an element in a hit-or-miss transform is exclusively foreground, background, or DNC. We propose two algorithms, one with single SE incorporating only the non-intersecting condition and another with two SEs incorporating both the non-intersecting condition and DNC.

*Single SE hit-or-miss transform:* Let  $f$  be an image and  $w$  be an SE. The SE elements are partitioned into  $w_h$  and  $w_m$  such that their pairwise intersection is empty, where  $w_h = \{w : w \leq 0\}$  and  $w_m = \{w : w \geq 0\}$ . The hit-or-miss neuron is defined as

$$(f \odot w)(x, y) = \min_{a, b \in D_{w_h}} (f(x + a, y + b) + w_h(a, b)) - \max_{c, d \in D_{w_m}} (f(x + c, y + d) + w_m(c, d)), \quad (5)$$

where, for sake of this article,  $w_h$  and  $w_m$  conceptually correspond to foreground and background. This formulation has advantages: (i) implicit complementary conditions, (ii) fewer parameters, and (ii) fewer algebraic operations, thus less complexity and more computational efficiency. A caveat of this method is 0 acts as a transition point between foreground and background so DNC cannot be enforced around this transition point, which otherwise would hinder switching of foreground elements to background and vice versa.

*Dual SEs hit-or-miss transform:* Algorithm 1 outlines the proposed algorithm. The algorithm takes an input image, the size of the SEs, and the threshold for DNC. To enforce DNC and/or the non-intersecting condition, we take aid of two auxiliary variables,  $a_h$  and  $a_m$ , initialized with zeros. The elements not part of  $h$  and  $m$  are assigned to  $-\infty$  in  $a_h$  and  $a_m$ , respectively. Then the hit is calculated as  $\min(f - h - a_h)$  and miss as  $\max(f + m + a_m)$ .

Because of separate SEs for foreground and background, an element can switch back and forth from one to another without transitioning through DNC region. However, once an element falls below the threshold and enters into the DNC non-optimization space, it cannot revert owing to the gradient being zero in this space.

*Soft hit-or-miss (SHM):* Eq. (4) for the hit-or-miss transform involves max and min operations, which are extremely sensitive to small variation and fluctuation in the input image. A sudden fluctuation in just one pixel can change the output from a target shape being present to absent. Therefore, we propose an extension of the hit-or-miss transform, referred to

---

### Algorithm 1: The hit-or-miss transform using two SEs

---

- 1 Input: Image  $f$  and threshold for DNC,  $th$ .
  - 2 Initialize two matrices,  $h$  and  $m$  (hit and miss SEs), pseudo-randomly w.r.t. a half-normal distribution.
  - 3 Find the mask for DNC as the indices,  $I_D$  of  $D = \{x | x \geq \max(h, m) \text{ and } x \leq th\}$ .
  - 4 Find the mask of non-foreground elements in  $h$  as the indices,  $I_{A_h}$  of  $A_h = \{x | x \leq \max(h, m) \text{ and } x \in h\}$
  - 5 Initialize an auxiliary matrix  $a_h$  of the same size as  $h$  with 0's.
  - 6 Set  $a_h[I_D + I_{A_h}] = -\infty$
  - 7 Calculate  $hit = \min(f - h - a_h)$
  - 8 Find the mask of non-background elements in  $m$  as the indices,  $I_{A_m}$  of  $A_m = \{x | x \leq \max(h, m) \text{ and } x \in m\}$
  - 9 Initialize an auxiliary matrix  $a_m$  of the same size as  $m$  with 0's.
  - 10 Set  $a_m[I_D + I_{A_m}] = -\infty$
  - 11 Calculate  $hit miss = \max(f + m + a_m)$
  - 12 Calculate the hit-or-miss transform as  $f \odot (h, m) = hit + miss$ ,
- 

herein as *soft hit-or-miss* (SHM), using a parametric soft-max and soft-min in place for max and min, respectively.

$$(f \odot^s (h, m))(x, y) = \text{softmin}_{a, b \in D_{h_f}} (f(x + a, y + b) - h(a, b)) - \text{softmax}_{a, b \in D_{m_b}} (f(x + a, y + b) + m(a, b)), \quad (6)$$

subject to

$$h(a, b) \geq m^c(a, b), \text{ or } m(a, b) \geq h^c(a, b).$$

While there exists several formulae to define soft-min and soft-max, herein we opt for a generalized mean based on smooth-max function parameterized by  $\alpha$ ,

$$s_\alpha(x) = \frac{\sum x e^{\alpha x}}{\sum e^{\alpha x}}, \quad (7)$$

where  $\alpha \in \mathbb{R}$ . This has an advantage over other generalized mean equations such as power and Lehmer means that it produces real valued output for non-negative valued inputs when fractional exponent is used whereas power and Lehmer means produce complex-valued results. Based on Eq. (7), the softmax and softmin operators are defined as

$$\text{softmax} = s_{smax, \alpha}(x) = \{s_\alpha(x) | \alpha \geq 0\},$$

$$\text{softmin} = s_{smin, \alpha}(x) = \{s_{-\alpha}(x) | \alpha \geq 0\}.$$

### C. The hit-or-miss transform inspired generalized convolution

In this section, we show that like the hit-or-miss transform, convolution also considers both foreground and background of a target structure. The difference is that an SE in hit-or-miss encodes absolute level of target shape whereas a filter in convolution encodes relative importance/level. As a result, the hit-or-miss transform can provide an absolute measure of how the target shape fits in an image whereas convolution provides relative measure of correlation or the degree of matching. The hit-or-miss transform can tell us whether an image fits a target pattern and the minimum offset between target shape and image. For example, perfect alignment will produce a value

of 0 in the hit and  $-1$  in the miss for an image with input in an unit interval (as illustrated with an example in Fig. 2). On the other hand, convolution will produce higher output for an image with target than non-target, so just looking at the convolution output, we cannot say whether a target shape is present in the image or not.

Given an image  $f$ , the convolution operation on this image w.r.t. a filter  $w$  is

$$(f * w)(x, y) = \sum_{a, b \in D_w} f(x - a, y - b) w(a, b)$$

This equation can be decomposed into two parts with positive and negative weights, respectively.

$$(f * w)(x, y) = \sum_{(a, b) \in D_{w_h}} f(x - a, y - b) w_h(a, b) - \sum_{(c, d) \in D_{w_m}} (-1)f(x - c, y - d) w_m(c, d), \quad (8)$$

where  $w_h = \{w : w > 0\}$  and  $w_m = \{w : w < 0\}$ . It is worth noting the structural similarity of hit and miss terms with those in the hit-or-miss transform. Since  $f * w$  increases with increasing coefficient of  $w_h$  and decreasing coefficient of  $w_m$ ,  $w_h$  and  $w_m$  indicate the weight or the relative importance of the foreground and background elements of the target pattern, respectively. As such, non-negative weights are hit (foreground), non-positive weights are miss (background), and zeros act as DNC in convolution. Following the convention in CNN, we do not flip image or filter in our implementation of convolution.

The linear operation, sum, in Eq. 8, gives equal importance to all operands regardless of their values. Instead, we can use soft-min for the foreground in the first term so that those with smallest values dominate the results (akin to erosion). Similarly, the sum for the background/miss can be generalized with a soft-min operation so that those with largest values in the local neighborhood dominate the results (akin to dilation). We refer to this extension as *generalized convolution 1* (GC1), denoted  $*^{g1}$ .

$$(f *^{g1} w)(x, y) = n(s_{smin, \alpha_1}(f(x - a, y - b) w_h(a, b)) - s_{smax, \alpha_2}((-1)f(x - c, y - d) w_m(c, d))), \quad (9)$$

or

$$(f *^{g1} w)(x, y) = n(s_{smin, \alpha_1}(f(x - a, y - b) w_h(a, b)) + s_{smin, \alpha_2}(f(x - c, y - d) w_m(c, d))) \quad (10)$$

where  $s_{smin, \alpha_1}$  and  $s_{smax, \alpha_2}$  are the softmax and softmin aggregation operations spanning between mean and maximum and between minimum and mean, respectively. Note that we apply a multiplication factor  $n$  in Eqs. (9) and (10) so that it becomes convolution when  $\alpha = 0$ . Eq. (10) has the computational advantage over Eq. (9) as it requires computation only of the soft-min whereas Eq. 9 involves both soft-max and soft-min.

We propose an alternative definition of the generalized convolution that instead of decomposing the convolution operation analogous to the hit-or-miss transform, applies soft-max and

soft-min directly to the standard convolution and then takes their sum,

$$(f *^{g2} w)(x, y) = n(s_{smin, \alpha_1}(f(x - a, y - b) w(a, b)) + s_{smax, \alpha_2}(f(x - a, y - b) w(a, b))). \quad (11)$$

We refer to this operation as *generalized convolution 2* (GC2). Next, we discuss how this extension will affect the gradient-descent based optimization, more specifically initialization.

*Optimization:* Recent advancements and key insights into the optimization process of a neural network such as initialization, skip connection in a residual network, and batch normalization contributed to achieving high performance. Kaiming He et al. [32] showed that initializing weights such that the variance of the output of a layer remains the same as the input helps to keep the distribution of gradients unvaried across all layers. This addresses the vanishing gradient problem, enabling training of a very deep neural network. However, their analysis was limited to convolution with ReLu activation function.

Convolution involves sum and product, both of which are linear operations and have closed form equations for variances (e.g., sum of variances for sum and product of variances for product). In contrast, there is no similar closed-form equation for max/min and generalized mean. Therefore, we model the variance in the form of  $\sigma_{s, \alpha}^2 = an^b \sigma_x^2$  for different values of  $\alpha$ , where  $n$  is the number of elements in a SE, and  $a$  and  $b$  are learned. We used a synthetic dataset where  $x$  is generated pseudo-randomly from a Gaussian distribution with unit variance and  $n = [3 \ 6 \ 9 \dots 24]^2$ . Table II lists the ratio of the input and output variances of Eq. 7 for different  $\alpha$ .

TABLE II: Variance of the smooth-max function,  $s_\alpha$  vs.  $\alpha$

$\alpha$	0	$\pm 0.5$	$\pm 1$	$\pm 2$	$\pm \infty$ (max/min)
$\sigma'_{s_\alpha} (= \sigma_{s_\alpha}^2 / \sigma_x^2)$	$\frac{1}{n}$	$\frac{1.32}{n^{0.95}}$	$\frac{1.44}{n^{0.74}}$	$\frac{0.82}{n^{0.32}}$	$\frac{0.60}{n^{0.24}}$

Another challenge with finding the exact criteria for initialization is the interdependency of terms. As we know, the variance of  $z = x \pm y$  is  $\sigma_z^2 = \sigma_x^2 + \sigma_y^2 \pm 2\sigma_{xy}^2$ , where  $\sigma_{xy}^2$  is the covariance between  $x$  and  $y$ . When  $x$  and  $y$  are independent, their covariance will be zero, and the variance of  $z$  can be obtained directly by summing up the variance of individual components. However, this is not the case for hit-or-miss transform (e.g., Eq. (4)) and extensions (e.g., Eq. (10)), where  $f$  exists in both hit and miss terms. Since  $\alpha$  changes the distribution, which in turn changes the covariance, the analysis is very complicated. Herein, we simplify the variance analysis by ignoring the covariance term and using modeled equations for the generalized mean. The Appendix provides initialization criteria for extensions of hit-or-miss transforms and convolution, which can be applied to standard operations as well.

#### IV. EXPERIMENTS

In order to compare our proposed algorithms with its standard counterparts, we consider both synthetic and real datasets. The synthetic dataset consists of a simple classification task

with two fixed-shape objects that all the methods can correctly classify all objects with a single layer, thus allowing us to visualize and interpret the learned SEs and shed lights onto the inner workings of these algorithms.

We evaluate the performance of our proposed algorithms in terms of classification accuracy on two benchmark datasets with varying context, shape, and size—from approximately fixed-sized, and rigid shaped objects with constant background in Fashion-MNIST to complex background, varied sized, and shaped objects in Cifar-10.

Since our focus is to compare different feature learning operations rather than other aspects of deep learning such as architecture or optimization algorithms, we select a small VGG-like [33] architecture with 4 layers, referred to as mini-VGG (see Table III for its architecture). This small NN also allows us to have the same setup (e.g., hyper-parameters and optimization algorithm) for all experiments, including convolution and standard hit-or-miss. First, we provide an analysis of different initialization strategies followed by experiments on hit-or-miss transform and convolution and their extensions.

TABLE III: Mini-VGG (4 layer NN)

Layer	Filter size
Input layer	28 × 28 × 1 (MNIST/Fashion-MNIST)
	32 × 32 × 3 (Cifar-10)
HMC <sup>1</sup> layer + BN <sup>2</sup> + ReLU <sup>3</sup>	3 × 3 × 32, padding=1
HMC <sup>1</sup> layer + BN + ReLU	3 × 3 × 32, padding=1
MaxPool	2 × 2
Dropout	25%
HMC <sup>1</sup> layer + BN + ReLU	3 × 3 × 64, padding=1
HMC <sup>1</sup> layer + BN + ReLU	3 × 3 × 64, padding=1
MaxPool	2 × 2
Dropout	25%
Fully Connected Layer + BN + ReLU	512
Dropout	50%
Softmax layer	10

<sup>1</sup> HMC denotes the basic operation specific to a particular network, e.g., convolution in CNN and hit-or-miss in morphological NN;

<sup>2</sup> Batch-Normalization;

<sup>3</sup> Rectified Linear Unit.

#### A. Synthetic dataset

This dataset consists of two objects, a solid circle and an annular ring with a hollow at the center, on a 28 × 28 grid, as shown in the leftmost column in Fig. 3. Two hundred images from each class were generated by perturbing these images with a Gaussian noise with a standard deviation of 0.03. A single layer NN with two 28 × 28 hit-or-miss transform/convolution filters without padding was batch-optimized using gradient descent with a learning rate of 0.01 and momentum 0.9 for 1000 epochs. The network was initialized with a fixed 0.01 for DF hit-or-miss transforms; and −0.01 and 0.01 for convolution and SF hit-or-miss transform. We used the mean of squared error as the loss function.

Fig. 3 shows the learned filters/SEs. Since convolution itself is a linear operation, we also included convolution+ReLU to make it non-linear and thus comparable to non-linear hit-or-miss transforms. As we can see, convolution+ReLU learns the shape of only one class, annular ring, with foreground shape,

hollowed ring, for the hit, and a solid circle the same size as the hole in the ring for the miss. The filters for the solid circle class are just the opposite of those for the annular ring. In effect, convolution decides based on whether a ring is present or absent in an input image, acting as a relative measure rather than finding a similarity measure with corresponding object shape. Contrast these filters against those SEs for the standard hit-or-miss transform. The learned shapes are now consistent with the class objects, e.g., circle and inverted circle for the hit and miss for solid circle object; and ring and inverted ring for the annular ring object. Enforcing the non-intersecting condition helps to learn the solid circle better and the annular ring worse. Adding DNC makes the filters sparse. The SF hit-or-miss transform yields very sparse SEs, e.g., SEs for the solid circle includes some dots close to the center in the hit and on the outer-side in the miss, and are sufficient to detect a solid circle. Note that due to the discriminatory nature of learning, exact matching is not required to obtain a peak classification accuracy. Therefore, the speckles within the SEs/filter may be relevant and can be robust against noise and imperfection in the input image.

#### B. Benchmark datasets

We first provide a brief description of the datasets used in this experiment.

*a) Fashion-MNIST:* This data set consists of fashion articles images of 10 classes; t-shirt/top, trouser, pullover, dress, coat, sandal, shirt, sneaker, bag, and ankle boot. This dataset is similar to the MNIST in term of number of examples, image size, and training-test partition, and number of classes.

*b) Cifar-10:* This data set consists of 60000 32 × 32 colour images in 10 classes, with 6000 instances per class. The dataset is partitioned into training and test with 50,000 and 10,000 examples, respectively.

*1) Impact of initialization:* We consider three distributions, uniform, normal, and half-normal, with different parameters. We optimize miniVGG with standard hit-or-miss transform for 70 epochs using Adam optimization [34] with a learning rate of 0.001 and a batch size of 64. The best test classification accuracy for each experiment is reported in Table IV.

As seen in Table IV, initialization can make a big difference. For example, using a normal instead of uniform distribution increases the accuracy by 20% on Cifar-10 dataset. Half-normal distribution boosts the performance further by 3.61%. This improvement can be explained by the fact that normal distribution has a high density around the mid-point. In contrast, half-normal has a high density at the lower end, thus facilitating sparse optimization as fewer elements will contribute to the error. Adopting the initialization condition put forth in Appendix B gives the best result.

*2) hit-or-miss transform and convolution:* The experiment setup is the same except that 150 epochs is used versus 70 in prior experiments. We used Kaiming initialization [32] for convolution. For DNC, we used threshold,  $th = 0.0$ .

As seen in Table V, foreground aka hit is a better predictor (56% accuracy on Cifar-10) than background aka miss (53.1%). Standard hit-or-miss transform improves the performance further by 16.16% demonstrating the importance of

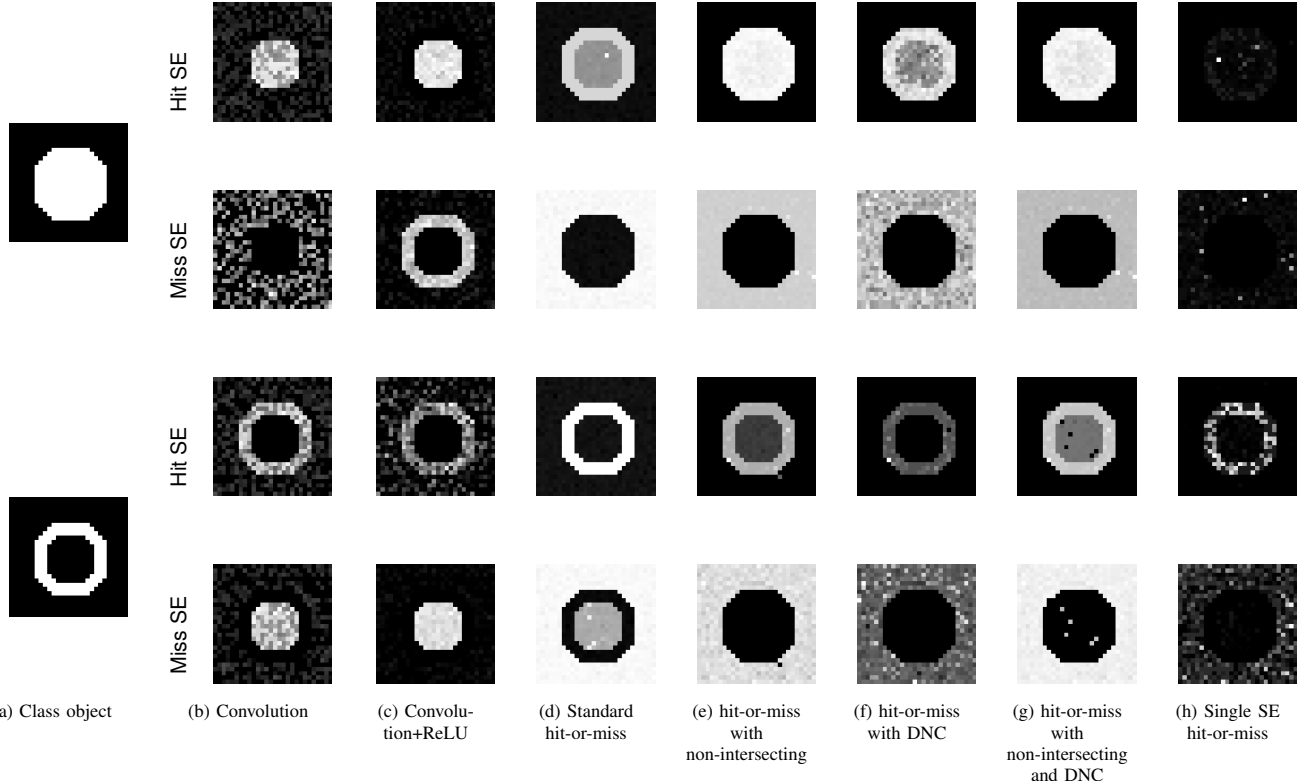


Fig. 3: Visualization of the learned SEs and filters for synthetic objects. Convolution+ReLU learns the shape of one object, annular ring, and uses it and its invert to discriminate between the two objects. On the other hand, hit-or-miss learns the shapes of both objects. Speckles within the filters may be relevant as the exact matching is not required to obtain a peak classification accuracy due to the discriminatory nature of learning and can be robust against noise and imperfection in the input images.

TABLE IV: Results for different initialization strategies for standard hit-or-miss transform

Distribution	Parameter	Datasets	
		Fashion-MNIST	Cifar-10
Uniform	U(-0.01,0.01)	89.33	32.54
	U(-1,1)	90.26	44.83
Normal	N(0,0.1)	89.13	57.12
	N(0,1)	91.56	64.15
Half-normal	HN(0,1)	92.4	67.76
	According to Appendix. B	92.48	69.57

both foreground and background in object detection. However, accuracy remains more-or-less the same for the the proposed method after incorporating the non-intersecting condition and DNC. Several factors affect the performance: (i) adding the non-intersecting condition makes the optimization problem more constrained that weakens its approximation power to learn an arbitrary function, and (ii) DNC space is discontinuous, where no updating occurs during optimization, limiting its ability to learn proper SEs.

While the hit-or-miss transform enables learning interpretable SE, convolution outperforms all variants of hit-or-miss

TABLE V: Results for hit-or-miss transforms and convolution

Methods	Constraints	Fashion-MNIST	Cifar-10
Hit (Erosion)		90.97	56.33
Miss (-Dilation)		88.33	53.10
Dual SEs hit-or-miss	None	93.31	72.49
	Non-intersecting	93.25	72.72
	DNC ( $th=0.0$ )	93.25	72.91
	Non-intersecting + DNC ( $th=0.0$ )	93.25	72.72
Single SE hit-or-miss		93.09	72.90
Convolution		<b>94.60</b>	<b>87.59</b>

transform. This performance gain by convolution is due in part to its superior ability to approximate an arbitrary function, as stated by the universal approximation theorem. So, one can trade-off between interpretability and accuracy and select an appropriate operation appropriate for a task.

3) *SHM and GC*: Table VI reports the results for extensions of the hit-or-miss transform and convolution. Relaxing max/min in the hit-or-miss transform with softer average-weighting operator enhances SHM's performance, though still lags behind standard convolution. GC1 results are at the

TABLE VI: Results for extensions of the hit-or-miss transform and convolution

Method	$\alpha$	Fashion-MNIST	Cifar-10
Dual SEs SHM	1.0	93.74	77.57
Dual SEs SHM + non-intersecting	1.0	93.75	77.39
Dual SEs SHM + DNC	1.0	93.64	77.32
Dual SEs SHM + non-intersecting + DNC	1.0	93.78	77.7
Single SE SHM	1.0	93.46	76.95
GC1	0.5	94.28	87.28
	1.0	94.32	87.76
Convolution with sum replaced by softmax (1st term of Eq. (11))	0.5	94.36	87.59
Convolution with sum replaced by softmax (2nd term of Eq. (11))	0.5	94.44	86.49
GC2	0.5	94.58	<b>88.29</b>
	1.0	<b>94.66</b>	87.71

same level as convolution. GC2 leads the scoreboard with an accuracy of 94.66 for Fashion-MNIST and 88.29 for Cifar-10. These results indicate that extensions in general boost the results, which reach maximum somewhere between  $\alpha = 0$  and  $\pm\infty$ .

All these experiments share a common story that convolution and the hit-or-miss transform come very close in terms of accuracy for simpler classification tasks (Fashion-MNIST) but the gap becomes wider for challenging tasks with complex objects (Cifar-10). There are many factors behind this performance gap, however the primary reasons can be attributed to (i) its underlying theory of measuring absolute fitness, which enables learning explainable filters but works as a hindrance in achieving top performance, and (ii) the difficulty of optimization with DNC.

## V. CONCLUSION AND FUTURE WORK

In this article, we provided an in-depth analysis of the theory of grayscale morphology, shedding some critical insights into its limitations and strengths. We also explored an application of a morphological operation, namely the hit-or-miss transform, that takes into account both foreground and background in measuring the fitness of a target pattern in an image. Unlike binary morphology, conventional grayscale morphological operations consider all pixels regardless of their relevance to a target shape. Furthermore, the SEs for hit and miss should be non-intersecting but not considered in the standard definition. Therefore, we propose to enhance the hit-or-miss transform accounting for these properties.

We outlined an optimization problem to appropriately learn semantically meaningful and interpretable SEs. Following this formulation, we provided two algorithms for the hit-or-miss transform with one and two SEs. Since max and min in the hit-

or-miss equation are too restrictive and overly sensitive to variation and fluctuation in inputs, we relaxed these operators with a parametric generalized mean, yielding a flexible and more powerful transform that leads to better classification accuracy. In the same spirit, we also extend the convolution, which outperforms standard convolution on benchmark datasets.

Our analysis and experimental results show that both the hit-or-miss transform and convolution consider both background and foreground, however they differ in the respect that the former provides an absolute measure while the latter gives a relative measure. These differences impact their ability in terms of interpretability and robustness. As better interpretability comes from an absolute measure, morphology leads convolution in this regard. On the other hand, relative measures are more robust so convolution outperforms morphology in classification accuracy.

We limit the focus of the current article to applying morphological operation in deep learning. In the future, we will study how to explain a morphological neural network solely based on the SEs leveraging the shapes learned by them. Furthermore, we will study how to better handle the discontinuity for DNC. Specifically we will explore other optimization techniques such as genetic algorithms (not stochastic gradient descent-based) with better constraints handling mechanism that will be able to update elements in a bidirectional manner across disjointed spaces. Finally, the initialization criteria developed herein was based on curve-fitting and simplified analysis. A future research direction can be toward conducting rigorous mathematical analysis to find exact closed-form equations for variances and co-variances involving generalized mean to enhance the performance further.

## APPENDIX

### A. GC2

Consider a NN layer consisting of GC2,

$$y = f * g^2 w = n (s_{smax, \alpha_1}(fw) + s_{smin, \alpha_2}(fw)),$$

followed by Relu activation function

$$z = \max(y, 0).$$

Let  $\sigma_f^2$  and  $\sigma_w^2$  be the variances of  $f$  and  $w$ , respectively. Ignoring the covariance between two terms, the variance of the output  $y$  will approximately be

$$\sigma_y^2 \approx n^2 \sigma_{s_{smax, \alpha_1}}'^2 \sigma_f^2 \sigma_w^2 + \sigma_{s_{smin, \alpha_2}}'^2 \sigma_f^2 \sigma_w^2$$

If we use symmetric soft-max and soft-min, function, then  $\alpha_1 = \alpha_2 = \alpha$  and  $\sigma_{s_{smax, \alpha_1}}^2 = \sigma_{s_{smax, \alpha_2}}^2 = \sigma_{s_\alpha}^2$ . This gives

$$\sigma_y^2 \approx 2n^2 \sigma_f^2 \sigma_w^2 \sigma_{s_\alpha}^2.$$

Since  $\sigma_z^2 = 0.5\sigma_y^2$  as shown in [32] for a symmetric distribution of  $y$ , As a result

$$\sigma_z^2 \approx n^2 \sigma_f^2 \sigma_w^2 \sigma_{s_\alpha}^2.$$

The output variance  $\sigma_z^2$  will be the same as  $\sigma_f^2$  if

$$\sigma_w^2 \approx \frac{1}{n^2 \sigma_{s_\alpha}^2},$$

which gives us the variance to initialize the filter weights. GC1 is also initialized with this same variance, which we found to give better results.

### B. Soft hit-or-miss transform

Consider a NN layer consisting of softer extension of standard hit and miss transform,

$$f \odot^s (h, m) = s_{smin, \alpha}(f - h) - s_{smin, \alpha}(f + m),$$

followed by Relu activation function

$$z = \max(y, 0).$$

Let  $\sigma_h = \sigma_m$ . Then  $\sigma_z^2 \approx \sigma_{s, \alpha}^2 (\sigma_f^2 + \sigma_h^2)$ . The condition for  $\sigma_z^2$  to be equal to  $\sigma_f^2$  is

$$\sigma_h^2 = \sigma_m^2 \approx \left( \frac{1}{\sigma_{s, \alpha}^2} - 1 \right) \sigma_f^2.$$

If initialized with half-normal distribution, then the variance will be,

$$\sigma_h^2 = \sigma_m^2 \approx \frac{1}{\sigma_{hn}^2} \left( \frac{1}{\sigma_{s, \alpha}^2} - 1 \right) \sigma_f^2,$$

where  $\sigma_{hn}$  is the ratio of half-normal to normal variances,  $\sigma_{hn}^2 = (1 - 2/\pi)$ .

We use this variance to initialize both standard and proposed hit-or-miss transforms. For  $|\alpha| < \infty$ , the variance obtained using this equation is very high, causing exploding gradient. To alleviate this, we scale the hit-or-miss transform equation with  $\sigma_{s, \infty}/\sigma_{s, \alpha}$  and initialize SEs the variance for  $\alpha = \pm\infty$ .

## REFERENCES

- [1] J. T. Springenberg, A. Dosovitskiy, T. Brox, and M. Riedmiller, "Striving for simplicity: The all convolutional net," *arXiv preprint arXiv:1412.6806*, 2014.
- [2] K. Simonyan, A. Vedaldi, and A. Zisserman, "Deep inside convolutional networks: Visualising image classification models and saliency maps," *arXiv preprint arXiv:1312.6034*, 2013.
- [3] D. Mellouli, T. M. Hamdani, J. J. Sanchez-Medina, M. B. Ayed, and A. M. Alimi, "Morphological convolutional neural network architecture for digit recognition," *IEEE transactions on neural networks and learning systems*, 2019.
- [4] S. Halkiotis, T. Botsis, and M. Rangoussi, "Automatic detection of clustered microcalcifications in digital mammograms using mathematical morphology and neural networks," *Signal Processing*, vol. 87, no. 7, pp. 1559–1568, 2007.
- [5] Y. Won and P. D. Gader, "Morphological shared-weight neural network for pattern classification and automatic target detection," in *Proceedings of ICNN'95-International Conference on Neural Networks*, vol. 4. IEEE, 1995, pp. 2134–2138.
- [6] Y. Won, P. D. Gader, and P. C. Coffield, "Morphological shared-weight networks with applications to automatic target recognition," *IEEE Transactions on neural networks*, vol. 8, no. 5, pp. 1195–1203, 1997.
- [7] H. Zheng, L. Pan, and L. Li, "A morphological neural network approach for vehicle detection from high resolution satellite imagery," in *International Conference on Neural Information Processing*. Springer, 2006, pp. 99–106.
- [8] H. K. Sulehria, D. I. Ye Zhang, and A. K. Sulehria, "Vehicle number plate recognition using mathematical morphology and neural networks," *WSEAS Transactions on Computers*, vol. 7, no. 6, pp. 781–790, 2008.
- [9] X. Jin and C. H. Davis, "Vehicle detection from high-resolution satellite imagery using morphological shared-weight neural networks," *Image and Vision Computing*, vol. 25, no. 9, pp. 1422–1431, 2007.
- [10] B. Raducanu, M. Grana, and P. Sussner, "Morphological neural networks for vision based self-localization," in *Proceedings 2001 ICRA. IEEE International Conference on Robotics and Automation (Cat. No. 01CH37164)*, vol. 2. IEEE, 2001, pp. 2059–2064.
- [11] P. D. Gader, M. A. Khabou, and A. Koldobsky, "Morphological regularization neural networks," *Pattern Recognition*, vol. 33, no. 6, pp. 935–944, 2000.
- [12] A. K. Hocaoglu and P. D. Gader, "Domain learning using choquet integral-based morphological shared weight neural networks," *Image and Vision Computing*, vol. 21, no. 7, pp. 663–673, 2003.
- [13] M. A. Khabou, P. D. Gader, and J. M. Keller, "Ladar target detection using morphological shared-weight neural networks," *Machine Vision and Applications*, vol. 11, no. 6, pp. 300–305, 2000.
- [14] N. Theera-Umporn, M. A. Khabou, P. D. Gader, J. M. Keller, H. Shi, and H. Li, "Detection and classification of mstar objects via morphological shared-weight neural networks," in *Algorithms for Synthetic Aperture Radar Imagery V*, vol. 3370. International Society for Optics and Photonics, 1998, pp. 530–540.
- [15] A. Oudou, "Vehicle detection using morphological shared-weight neural network in the multiple instance learning framework," Ph.D. dissertation, University of Missouri–Columbia, 2017.
- [16] B. Perret, S. Lefèvre, and C. Collet, "A robust hit-or-miss transform for template matching applied to very noisy astronomical images," *Pattern Recognition*, vol. 42, no. 11, pp. 2470–2480, 2009.
- [17] V. Chatzis and I. Pitas, "A generalized fuzzy mathematical morphology and its application in robust 2-d and 3-d object representation," *IEEE Transactions on Image Processing*, vol. 9, no. 10, pp. 1798–1810, 2000.
- [18] V.-T. Ta, A. Elmoataz, and O. Lézoray, "Nonlocal pdes-based morphology on weighted graphs for image and data processing," *IEEE transactions on Image Processing*, vol. 20, no. 6, pp. 1504–1516, 2010.
- [19] N. Bouaynaya and D. Schonfeld, "Theoretical foundations of spatially-variant mathematical morphology part ii: Gray-level images," *IEEE Transactions on pattern analysis and machine intelligence*, vol. 30, no. 5, pp. 837–850, 2008.
- [20] L. Ji and J. Piper, "Fast homotopy-preserving skeletons using mathematical morphology," *IEEE Transactions on Pattern Analysis & Machine Intelligence*, no. 6, pp. 653–664, 1992.
- [21] F. Zana and J.-C. Klein, "Segmentation of vessel-like patterns using mathematical morphology and curvature evaluation," *IEEE transactions on image processing*, vol. 10, no. 7, pp. 1010–1019, 2001.
- [22] E. R. Urbach, J. B. Roerdink, and M. H. Wilkinson, "Connected shape-size pattern spectra for rotation and scale-invariant classification of gray-scale images," *IEEE Transactions on Pattern Analysis and Machine Intelligence*, vol. 29, no. 2, pp. 272–285, 2007.
- [23] P. L. Palmer and M. Petrou, "Locating boundaries of textured regions," *IEEE transactions on geoscience and remote sensing*, vol. 35, no. 5, pp. 1367–1371, 1997.
- [24] R. M. Haralick, S. R. Sternberg, and X. Zhuang, "Image analysis using mathematical morphology," *IEEE transactions on pattern analysis and machine intelligence*, no. 4, pp. 532–550, 1987.
- [25] D. Sinha and E. R. Dougherty, "Fuzzy mathematical morphology," *Journal of Visual Communication and Image Representation*, vol. 3, no. 3, pp. 286–302, 1992.
- [26] K. Nogueira, J. Chanussot, M. D. Mura, W. R. Schwartz, and J. A. d. Santos, "An introduction to deep morphological networks," *arXiv preprint arXiv:1906.01751*, 2019.
- [27] P. D. Gader, Y. Won, and M. A. Khabou, "Image algebra networks for pattern classification," in *Image Algebra and Morphological Image Processing V*, vol. 2300. International Society for Optics and Photonics, 1994, pp. 157–168.
- [28] R. C. Gonzalez, R. E. Woods *et al.*, "Digital image processing," 2002.
- [29] E. R. Dougherty, "An introduction to morphological image processing," *SPIE*, 1992, 1992.
- [30] Y. LE CUN, "Constrained neural networks for unconstrained handwritten digit recognition," *Proc. Frontiers in Handwriting Recognition*, pp. 145–151, 1990.
- [31] M. A. Khabou, P. D. Gader, and J. M. Keller, "Morphological shared-weight neural networks: A tool for automatic target recognition beyond the visible spectrum," in *Proceedings IEEE Workshop on Computer Vision Beyond the Visible Spectrum: Methods and Applications (CVBVS'99)*. IEEE, 1999, pp. 101–109.
- [32] K. He, X. Zhang, S. Ren, and J. Sun, "Delving deep into rectifiers: Surpassing human-level performance on imagenet classification," in *Proceedings of the IEEE international conference on computer vision*, 2015, pp. 1026–1034.
- [33] K. Simonyan and A. Zisserman, "Very deep convolutional networks for large-scale image recognition," *arXiv preprint arXiv:1409.1556*, 2014.
- [34] D. Kingma and J. Ba, "Adam: A method for stochastic optimization," in *3rd International Conference for Learning Representations*, 2015.